Spring 5-2009

Composite Rotor Design for a Hydrokinetic Turbine

Seth Hunter Pierson
University of Tennessee - Knoxville

Senior Design Project

Composite Rotor Design for a Hydrokinetic Turbine

Sponsor:

The National Renewable Energy Laboratory

Team Members:

Kyle Honkonen
Seth Pierson
Danny Sale
John Tencer

Faculty Advisor:

Dr. Boulet

May 1, 2009

TABLE OF CONTENTS

1. INTRODUCTION

The objective of this report is to investigate how design tools and methods commonly used in the wind turbine industry can be applied to the design of hydrokinetic turbines. This report contains two main components: the first component focuses on hydrodynamic design aspects and the second component focuses on structural design aspects. Ultimately, the methodologies developed in the hydrodynamic and structural analyses are used together to design a horizontal-axis fixed-speed stall-regulated hydrokinetic turbine rotor.

This first component of this report describes the development WT_Perf_GA, which is a user-friendly, graphical-user-interface (GUI) windows based application which enables users to quickly and intuitively design stall-regulated wind and hydrokinetic turbine rotors. The WT_Perf_GA optimization method couples a blade-element-momentum performance code (WT_Perf) with a modern genetic algorithm to design optimal stall-regulated rotors. WT_Perf_GA doubles as a design tool for both wind and hydrokinetic turbines; however WT_Perf_GA will be discussed in context to hydrokinetic turbines for the remainder of this report. WT_Perf_GA is an optimization method which calculates the optimal chord, twist, and hydrofoil distributions which maximize the hydrodynamic efficiency while ensuring that the rotor produces an ideal power curve and avoids cavitation. Additional constraints within the optimization method ensure that the calculated blade shapes are structurally and hydrodynamically feasible. Later sections of this report describe how WT_Perf_GA was successfully used to design a stall-regulated hydrokinetic turbine rotor which has optimal hydrodynamic performance.

The second component of this report focuses on the development of a two-tiered structural analysis method for composite turbine blades. The first tier of the structural analysis calculates the span-variant structural properties of a composite blade which are required to withstand a given static loading. The second tier of the structural analysis determines the strains and stresses experienced by a specified composite layout. Using these structural analysis tools, a detailed lamina schedule and composite material was designed for the hydrodynamically optimal rotor produced by the WT_Perf_GA code.

2. BACKGROUND & DESIGN CONSIDERATIONS

Hydrokinetic turbines are a class of “zero-head” hydropower which use the kinetic energy of flowing water to drive a generator. Hydrokinetic turbines operate on many of the same principles as wind turbines and share similar design philosophies. The most notable difference is that the density of water is about 850 times greater than air so the energy in a given flow stream is much greater for a hydrokinetic turbine than for a wind turbine. However, average flow velocities for a tidal or river flow tend to be an order of magnitude lower than flow velocities at a good wind site. The net impact is that the Reynolds numbers tend to be in the same range for both wind turbines and hydrokinetic turbines, which allows for much of the same experimental airfoil/hydrofoil data to be used in the design process. Additionally, hydrokinetic turbines can be analyzed and designed using the same incompressible flow techniques used for wind turbines. But unlike wind turbines, hydrokinetic turbines must be designed to avoid cavitation, a condition in which low pressures on the hydrofoil’s surface can result in local boiling of the water and lead to accelerated wear and increased load uncertainty.

Stall-regulated turbines typically operate at a single nominal rotor speed, and the blades are fixed in place and do not adjust during operation. Stall-regulated turbines have blades which are cleverly designed and shaped to increasingly stall, i.e. induce flow separation, as the free stream velocity increases. Passive stall regulation is an effective method of shedding excess power which would overload the turbine generator and for reducing the forces acting on the blades at high flow speeds. An ideal stall-regulated turbine should operate at high efficiencies from its cut-in to rated flow speed, and then begin to hydrodynamically stall and maintain a constant power output as the flow speed approaches and exceeds the rated speed of the turbine. In addition, the constant power output should match as closely as possible the rated power of the generator in order to maximize energy production.

Hydrokinetic turbines typically operate in flow regimes where the flow direction is more predictable than for wind turbines and hence yaw mechanisms can be simplified or eliminated. Wind turbines have grown in size over the past decades, using larger rotors and taller towers to take advantage of the faster winds aloft and to maximize the use of plant infrastructure. In contrast, hydrokinetic turbines are limited in size by the dimensions of the channel they are placed in. Passively controlled fixed-speed stall-regulated hydrokinetic turbines are unlikely to attain an annual energy production (AEP) as high as actively controlled variable-speed variable-pitch turbines, which are common in the wind industry. However, fixed-speed stall-regulated rotors have the potential to be more reliable and less costly due to the absence of extra control mechanisms and fewer moving parts. Moreover, in environments that have less variability in flow conditions, such as rivers in comparison to tidal straits, the added complexity and cost of a variable-speed rotor and variable-pitch blades may not be economically justifiable.

3. HYDRODYNAMIC ANALYSIS

3.1 WT_Perf Blade-Element-Momentum Model

This rotor optimization code takes advantage of the National Wind Technology Center's existing wind turbine performance code WT_Perf [3] to use as the hydrodynamic model. WT_Perf relies on blade-element momentum (BEM) theory to predict the steady state performance of wind and hydrokinetic turbines.

BEM theory, an extension of actuator disk theory, is a combination of two different theories: conservation of momentum theory and blade element theory. Conservation of momentum theory refers to a control volume analysis of the forces at the rotor plane based on the conservation of linear and angular momentum. As the fluid passes through the rotor plane, conservation of momentum states that the loss of pressure or momentum through the rotor plane is caused by work done on the turbine blades by the moving fluid. Conservation of momentum theory then allows one to calculate the induced velocities in the axial and tangential directions from the momentum lost by the moving fluid. A flow field, characterized by the axial and angular induced velocities, is used to define the local flow conditions at the rotor hydrofoils.

Blade-element theory is an analysis of forces which assumes that the blades can be divided into many smaller elements which act independently of surrounding elements. Given the local flow conditions and the blade geometry, the hydrodynamic forces on these blade elements can be calculated. Blade-element theory then sums these elemental forces along the span of the blade to calculate the total forces and moments exerted on the turbine.

These two approaches are combined into BEM theory, which is used to relate the geometry of the rotor and the lift and drag characteristics of the rotor hydrofoils to the rotor's ability to extract power from a moving fluid. In addition, BEM theory makes the following assumptions:

- Incompressible, inviscid, and steady state flow field
- There is no cavitation
- Forces on the blades are determined only by the lift & drag characteristics of the blade's hydrofoil shape
- Blade elements operate as two-dimensional hydrofoils with no interaction between blade elements

Despite the limitations listed above, BEM theory has been widely used as a reliable model for predicting wind turbine performance, and even successfully to predict hydrokinetic turbine performance. BEM theory is generally attributed to Betz and Glauert. A more thorough explanation and derivation of the BEM governing equations can be found in many wind turbine design handbooks [4].

3.2 Introduction of Cavitation Constraint into BEM Theory

As long as cavitation is avoided the theory of BEM is assumed to be valid for an axial flow hydrokinetic turbine. A cavitation constraint was introduced into the WT_Perf model to ensure that the calculated outputs are valid.

The condition required to avoid the inception of cavitation is given by Eqn. 1 [5], where σ is the non-dimensional cavitation number and C_{Pmin} is the local minimum pressure coefficient of the hydrofoil. If the condition in Eqn. 1 does not hold true, then the local static pressure of the moving fluid has dropped to a value less than the vapor pressure, and the continuity of flow is broken by the formation of vapor bubbles, i.e. cavitation has begun.

Cavitation is highly dependent on the pressure distribution of the moving fluid around the hydrofoil. The pressure at a point on the surface of the hydrofoil is defined by the pressure coefficient, C_P. The values of the pressure coefficient are dependent on the angle of attack, Reynolds number, surface roughness, and shape of the hydrofoil. Pressure coefficients are typically measured in wind tunnel tests or can be calculated via numerical methods. The non-dimensional cavitation number, defined by Eqn. 2, takes into account the axial and tangential induced velocities at the rotor plane.

The local velocity at the rotor plane is given by Eqn. 3. Using the relation in Eqn. 1, the local velocity required to induce cavitation can be calculated via Eqn. 4. To ensure that the rotor does not experience cavitation, V_{loc} must never exceed or equal $V_{cavitate}$ at any location along the blade.

$$\sigma + C_{Pmin} \geq 0 \tag{1}$$

$$\sigma = \frac{P_{atm} + \rho g h + \frac{1}{2}\rho V_\infty^2 a(2-a) - \frac{1}{2}\rho(\Omega r a')^2 - P_V}{\frac{1}{2}\rho V_{loc}^2} \tag{2}$$

$$V_{loc} = \sqrt{[V_\infty(1-a)]^2 + [(\Omega r)(1+a')]^2} \tag{3}$$

$$V_{cavitate} = \sqrt{\frac{P_{atm} + \rho g h + \frac{1}{2}\rho V_0^2 a(2-a) - \frac{1}{2}\rho(\Omega r a')^2 - P_V}{-\frac{1}{2}\rho C_{Pmin}}} \quad (4)$$

3.3 Application of Stall-Delay Models

One of the simplifying assumptions of BEM theory is that spanwise flow along the blade is neglected, but in reality the presence of spanwise flow can cause significant augmentations in lift, drag, and pressure along the blade, especially near the blade root. WT_Perf_GA requires the lift, drag, and pressure coefficients of the hydrofoils as inputs. These lift, drag, and pressure coefficients are usually measured by testing airfoil sections in a wind tunnel, and there are many publications in which this data is readily available [6-8]. Because of the inability of non-rotating wind tunnel tests to simulate the influence of three-dimensional spanwise flow present in wind and hydrokinetic turbines, stall-delay models are used to apply corrections to the two-dimensional airfoil data. The application of 3D corrections to the 2D hydrofoil data can significantly increase the accuracy of the WT_Perf predictions for unyawed flows.

Accounting for stall-delay for stall-regulated rotors is especially important in being able to accurately predict the peak power and post-stall performance. Two different stall-delays models have been incorporated into WT_Perf_GA. The user has the choice to correct the lift and drag coefficients via the Selig/Du [X] or Eggers [X] stall-delay model. These stall-delay models have shown to increase the accuracy of BEM predictions, and the use of the appropriate stall-delay model is left to the user's discretion. At present, a suitable model to apply stall-delay corrections to the pressure coefficients was unavailable.

3.4 Verification of WT_Perf Hydrodynamic Model

In 2007, Verdant Power installed an array of six 35kW turbines in the East River of New York City to demonstrate hydrokinetic tidal technology. In cooperation with Verdant Power, the NWTC was able to begin validating the WT_Perf hydrodynamic model by modeling the Verdant Power 35kW Gen4 hydrokinetic turbine. The Verdant Power 35kW Gen4 turbine, shown in Fig. 1, is a fixed-speed stall-regulated turbine with a 5m rotor diameter.

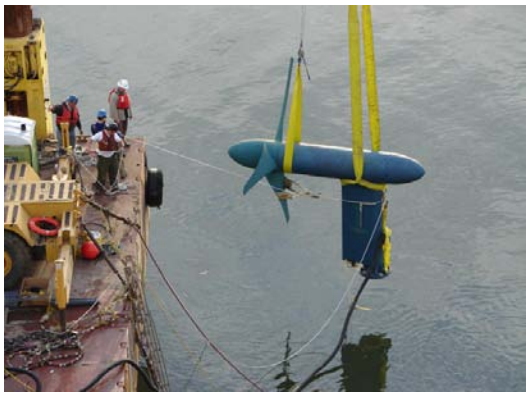

Figure 1. The Verdant Power 35kW hydrokinetic turbine.

Once the input parameters for the WT_Perf model were verified to accurately represent the existing Verdant Power turbine, the code's accuracy was verified by comparing the code's predictions to data measured from the Verdant Power turbine during full scale operation. The percent error between the measured and WT_Perf predicted mechanical power is shown in Fig. 2. Uncertainties in the measured data from the Verdant Power turbine were unavailable at the time, so in order to calculate the percent error, as shown in Fig. 2, an uncertainty of zero was assumed for the measured mechanical power. The WT_Perf model showed good agreement with the experimental data. It was observed that the accuracy of the WT_Perf model should be sufficient for use as a design tool for future hydrokinetic turbines.

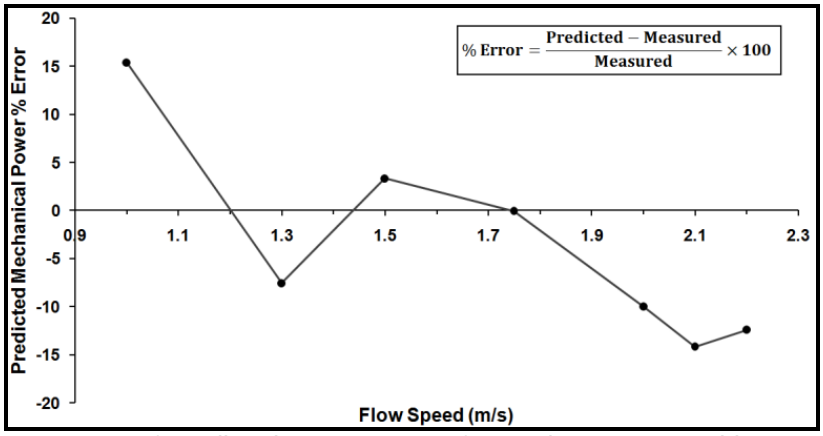

Figure 2. WT_Perf Predicted Power %Error for Verdant Power Turbine

4. WT_PERF_GA OPTIMIZATION CODE

4.1 WT_Perf_GA Overview

The design process for stall-regulated rotors involves many variables which often have complex trade-offs with each other. Performing trade studies between all possible design variations through traditional direct or iterative approaches is a time consuming and exhausting process. In addition, it may be possible that multiple optimal solutions exist and it can be difficult to distinguish which solution is truly the best—such studies are well suited to numerical optimization approaches. Traditional gradient based optimization methods (such as Newton's method) offer fast convergence times but can fail to converge on the global optimal solution in the presence of multiple minima/maxima. Although genetic algorithms (GA) converge much slower than gradient based methods, GAs hold a unique advantage in that they can effectively search the solution space and converge on a globally optimal solution by comparing and selecting the superior of all locally optimal solutions.

WT_Perf_GA couples a single objective genetic algorithm (GA) with the WT_Perf hydrodynamic model in a user friendly graphical-user-interface (GUI) that allows for rapid and intuitive design of optimal stall-regulated rotors. This rotor optimization code takes advantage of a modern GA developed by The MathWorks as part of the MATLAB Optimization Toolbox [12].

This optimization method calculates the optimal chord, twist, and hydrofoil distributions which maximize the hydrodynamic efficiency[1] while ensuring that the rotor produces an ideal power curve and avoids cavitation. Although WT_Perf_GA cannot select which hydrofoils should be used in the blade design, it can calculate an optimal placement of hydrofoils along the span of the blade when a family of hydrofoils (with corresponding lift, drag, & pressure coefficients) is input by the user. The hydrofoil distribution is modeled as a % thickness distribution, where the % thickness value determines which hydrofoil in the family—and thus which lift, drag, and pressure coefficients—are applied in the WT_Perf hydrodynamic performance model.

4.2 Formulation of Optimization Problem

To reduce the design parameters to a manageable number, the rotor diameter, rotor speed (rpm), and rated power are held constant in this optimization method. This optimization method defines 15 variables as the optimization variables, which together define the chord, twist, and % thickness distributions, as illustrated in Fig. 3. The chord, twist, and percent thickness distributions are each defined at five control points: the blade hub, the blade tip, and then at evenly spaced points in-between. To limit the amount of variables needed to completely define the blade geometry, Bezier curves are fit through the control points and WT_Perf is then evaluated at a sufficient resolution along the blade, as illustrated in Fig. 3. For structural and hydrodynamic motives, upper and lower bounds and inequality constraints are placed upon the chord, twist, and % thickness distributions such that each distribution decreases monotonically from the blade root to tip—this is done so that the calculated blade shapes are structurally and hydrodynamically feasible.

[1] Hydrodynamic efficiency is defined as the ratio of the mechanical power output at the input shaft to the total power available in the free stream flow.

In GA terminology, an individual is a vector containing values for the 15 optimization variables, and a set of individuals is called a population or generation. Figure 3 shows how an individual can define the complex three-dimensional shape of a turbine blade. The GA is initiated by creating an initial population of randomly generated individuals that satisfy the constraints of the problem and sufficiently sample the entire solution space. In this case, the initial population and all subsequent generations are subject to upper and lower bounds and inequality constraints such that the chord, twist, and % thickness variables are monotonically decreasing. These bounds and constraints on the control points allow the GA to converge on structurally and hydrodynamically feasible blade shapes without over-constraining the problem.

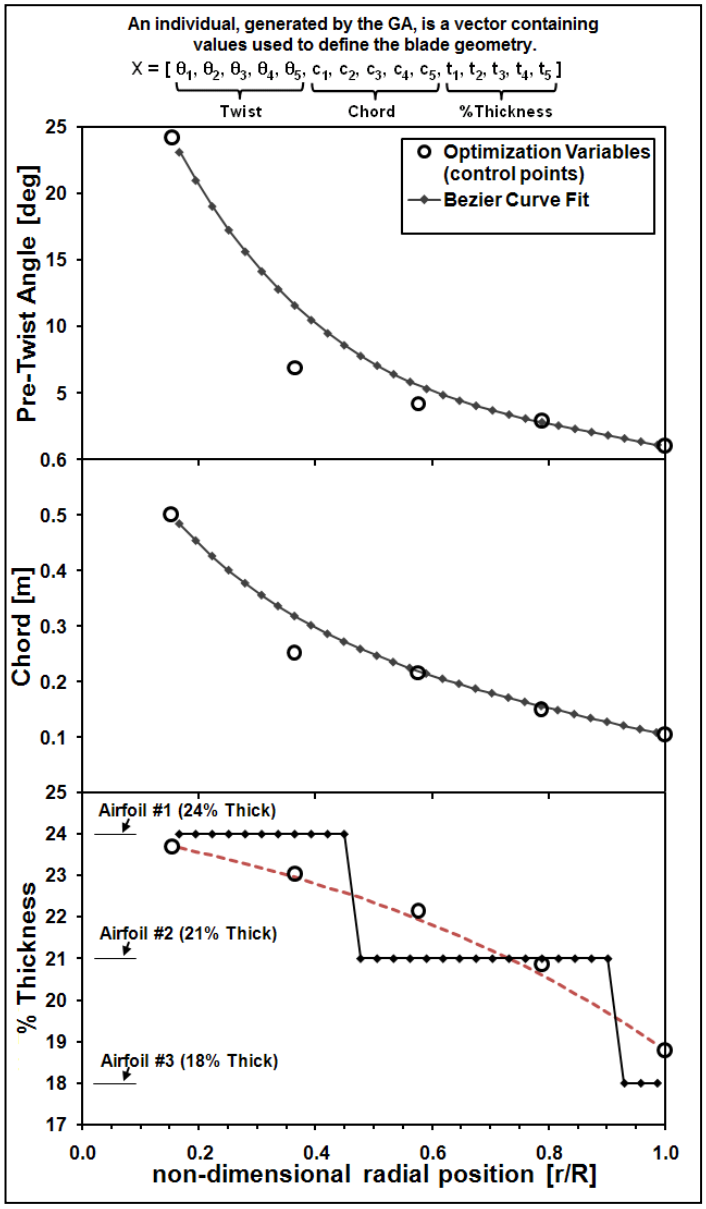

Figure 3 - The blade geometry distributions are each defined by a Bezier curve fit through the control points.

Each individual from the initial population represents a possible blade shape and is assigned a fitness value, which represents the degree to which the individual satisfies the rotor design criteria (i.e. achieves maximum hydrodynamic efficiency, achieves an ideal stall-regulated power curve, and avoids cavitation). In this method, the lowest fitness values represent optimal solutions which best satisfy the rotor design criteria and high fitness values represent blade shapes that performed poorly. The GA continues to search for individuals with the lowest (best) fitness values from one population to the next. The intelligence of the GA search algorithm comes from its ability to selectively allow individuals to reproduce—thus creating subsequent populations of potentially better performing individuals. Subsequent populations are generated as parent individuals reproduce with one another through the operations of crossover and mutation. Crossover is a reproductive function in which the child individual consists of varying proportions of identical traits from the parent individuals. Mutation is a reproductive function in which the child individual contains elements of the parent individual that have been randomly altered from their original state. By giving individuals with the lowest fitness values higher probabilities of being able to reproduce, subsequent populations can retain many of the best traits of individuals from previous generations and contain even better performing individuals. However, if succeeding populations of individuals are becoming too similar to each other, the GA can converge prematurely on non-optimal (local) solutions. Therefore, the diversity of succeeding generations is kept high through the use of crossover, mutation, and also by allowing poorly performing individuals to occasionally reproduce. This process of allowing individuals to reproduce from one generation to the next and searching for the lowest fitness value continues until either a blade shape is found which meets all the design specifications (i.e. has a sufficiently low fitness value) or until a maximum number of generations have been processed. Occasionally the genetic algorithm may produce blade shapes that experience cavitation or whose performance is so poor that the WT_Perf analysis will fail to converge—these individuals are assigned an arbitrarily high fitness value in order to decrease their chances of propagating into future generations. A flowchart of the WT_Perf_GA algorithm is illustrated in Fig. 4.

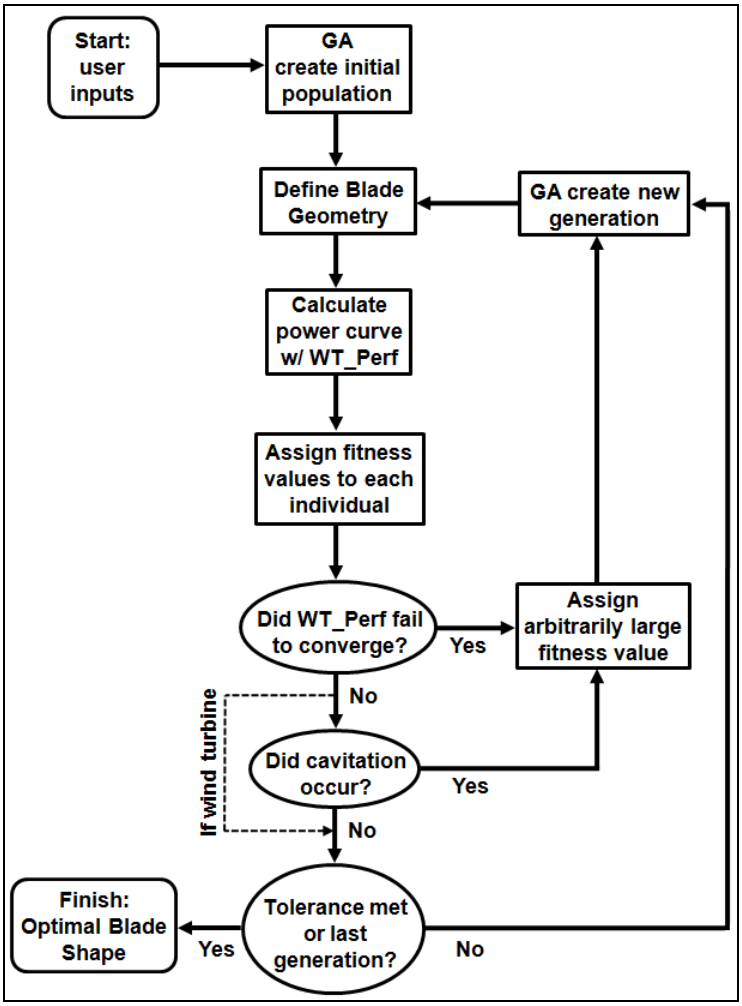

Figure 4. Flowchart of the WT_Perf_GA algorithm.

4.3 Defining an Optimal Solution

A fitness function is defined which allows the GA to mathematically determine if a blade shape sufficiently meets the design requirements. In this optimization method, an optimal stall-regulated rotor is one which produces an ideal power curve—i.e. the rotor should operate at high efficiencies from its cut-in to rated flow speed, and then begin to hydrodynamically stall and maintain a constant power output as the flow speed approaches and exceeds the rated speed of the turbine. The lowest fitness values are assigned to rotors which closely follow this ideal stall-regulated power curve. Evaluation of the fitness function is performed by WT_Perf—where each individual is passed to WT_Perf and assigned a fitness value.

The fitness function is defined by Eqn. 5, where $Area_1$ and $Area_2$ are defined by Eqns. 6 and 7, respectively. The values w_1 and w_2 are weight values specified by the user. However, experimentation has shown that the values of w_1 and w_2 have no noticeable effect on the optimization results or convergence rate—therefore WT_Perf_GA uses the default of $w_1=w_2=1$. Figure 5 further illustrates how the fitness function and its quantities of interest, $Area_1$ and $Area_2$, are defined.

$$F = w_1\,Area_1 + w_2 Area_2 \tag{5}$$

$$Area_1 = \int_{V_{cut-in}}^{V_{rated}} P_{Betz} - P_{turbine}\,dV_\infty \tag{6}$$

$$Area_2 = \int_{V_{rated}}^{V_{cut-out}} |P_{turbine} - P_{rated}|\,dV_\infty \tag{7}$$

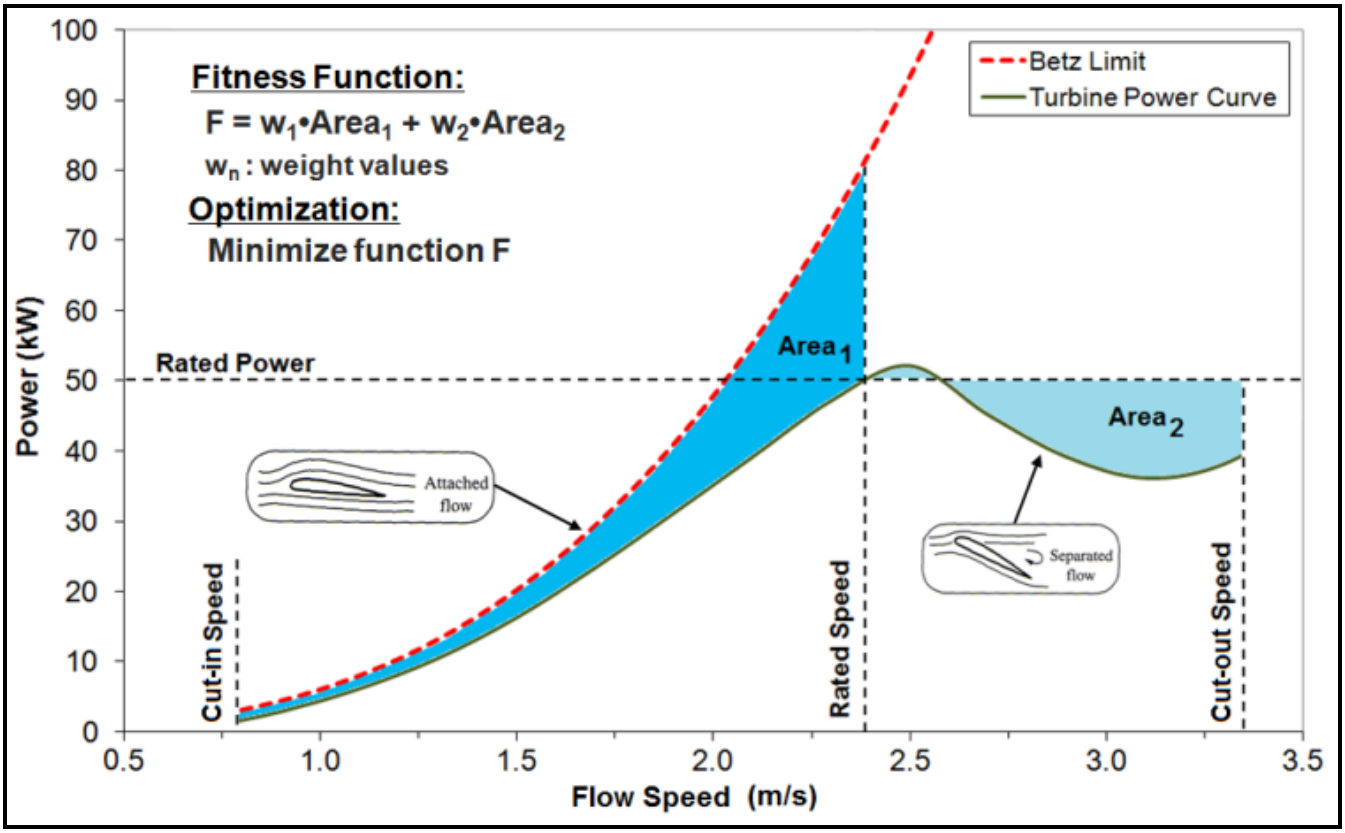

Figure 5. Example power curve for a stall-regulated turbine and definition of the fitness function and its quantities of interest.

The Betz limit is used as a practical upper limit on the highest efficiency attainable, and to maximize the efficiency of the turbine the area between the Betz limit and the turbine power curve ($Area_1$) is minimized. Optimizing a rotor for maximum hydrodynamic efficiency does not necessarily create a turbine with the lowest cost of energy (COE), but maximizing the efficiency is an excellent criterion to use as a first pass in the design process. An ideal stall regulated turbine would maintain a constant rated power output as the flow speed increases beyond the rated flow speed of the machine. Therefore, it is ideal to minimize the area between the line of rated power and the turbine power curve ($Area_2$). Therefore, within realistic bounds set upon the optimization variables, an optimal blade shape is found when $Area_1$ and $Area_2$ are minimized (i.e. the fitness function is minimized) and when cavitation is avoided.

Depending on the type of turbine being referred to, the term rated power can have varying definitions. However, in the context of this optimization method rated power refers to the constant power at which a stall-regulated turbine would ideally maintain at flow speeds exceeding the rated flow speed (i.e. in the post-stall region).

4.4 WT_Perf_GA Results

Figure 6 shows the twist, chord, % thickness, and thickness distributions for two rotors produced by WT_Perf_GA. The rotor labeled “Hydrodynamic Optimum” was output directly from the WT_Perf_GA code. Figure 7 is a screenshot of the WT_Perf_GA user’s interface and shows the input parameters that were used to generate the “Hydrodynamic Optimum” rotor. The “Hydrodynamic Optimum” blade shape was modified for structural considerations. The “Hydrodynamic Optimum” rotor was modified by hand to have a circular root, slightly extended radial length, and included a new more hydrodynamic tip shape—this modified rotor was renamed as “Structurally Improved”. The addition of these modifications, particularly the circular root, inherently changes the chord, % thickness, and thickness distributions as shown in Fig. 6.

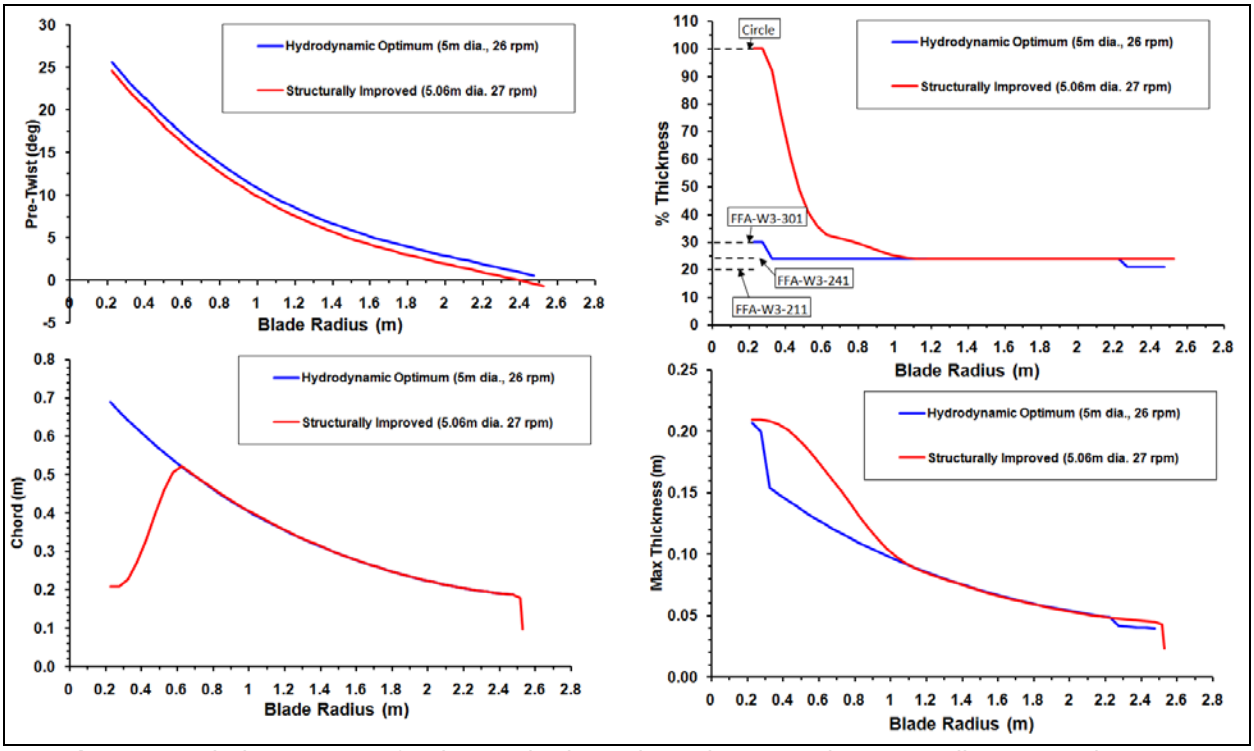

Figure 6 – Blade Geometry for the "Hydrodynamic Optimum" and "Structurally Improved" rotors.

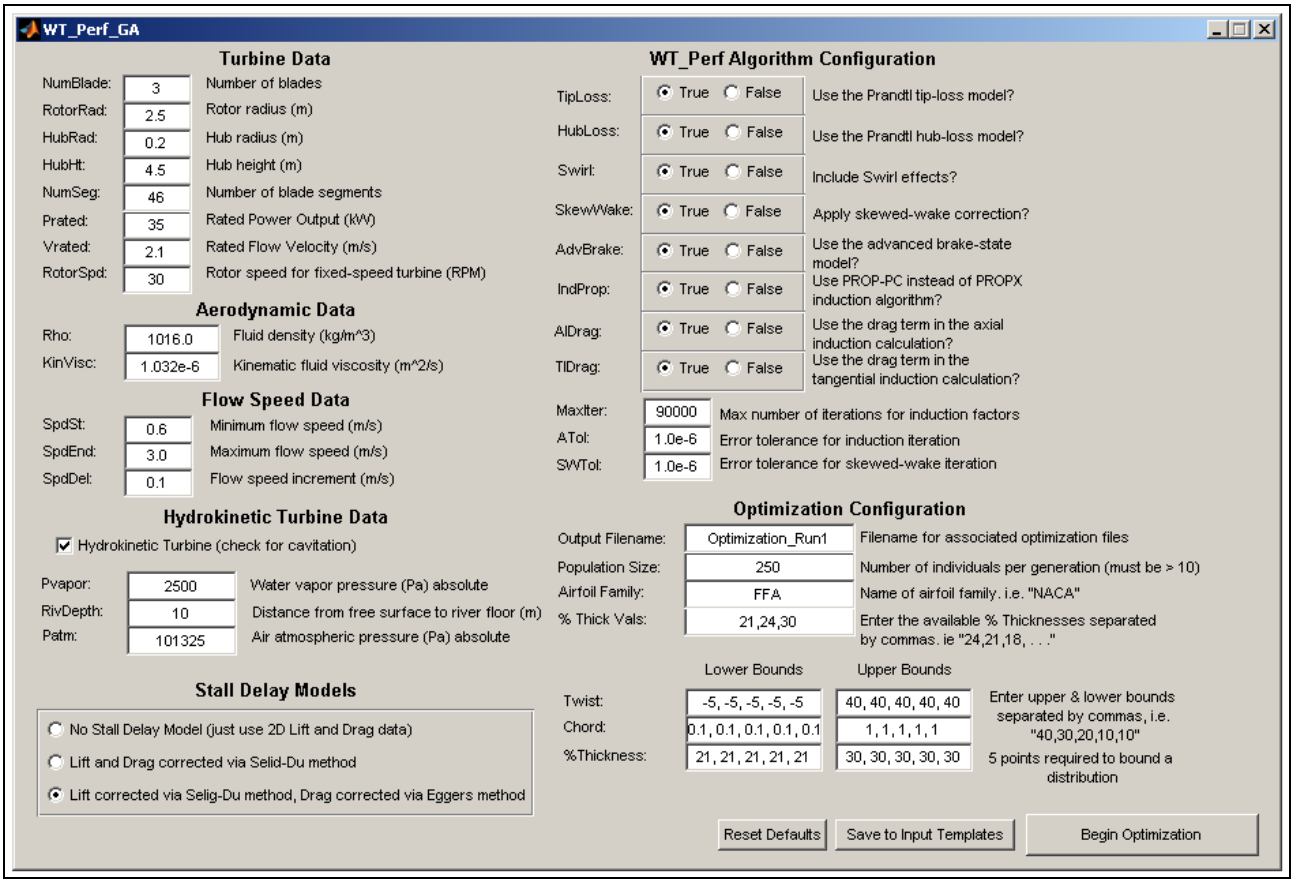

Figure 7 – Screenshot of the WT_Perf_GA user's interface, showing the input parameters used to generate the "Hydrodynamic Optimum" blade shape.

In order for the “Structurally Improved” rotor to achieve performance similar to the “Hydrodynamic Optimum” rotor produced by WT_Perf_Ga, the pre-twist was shifted by -1 degree, the rotor speed was increased from 26 to 27 rpm, and the diameter was increased from 5 to 5.06 meters. The power and efficiency curves for both blade shapes are shown in Fig. 8. The “Hydrodynamic Optimum” rotor performs with significantly higher efficiencies at low flow speeds, but both designs exhibit overall high efficiencies, as well as the desired stall characteristics.

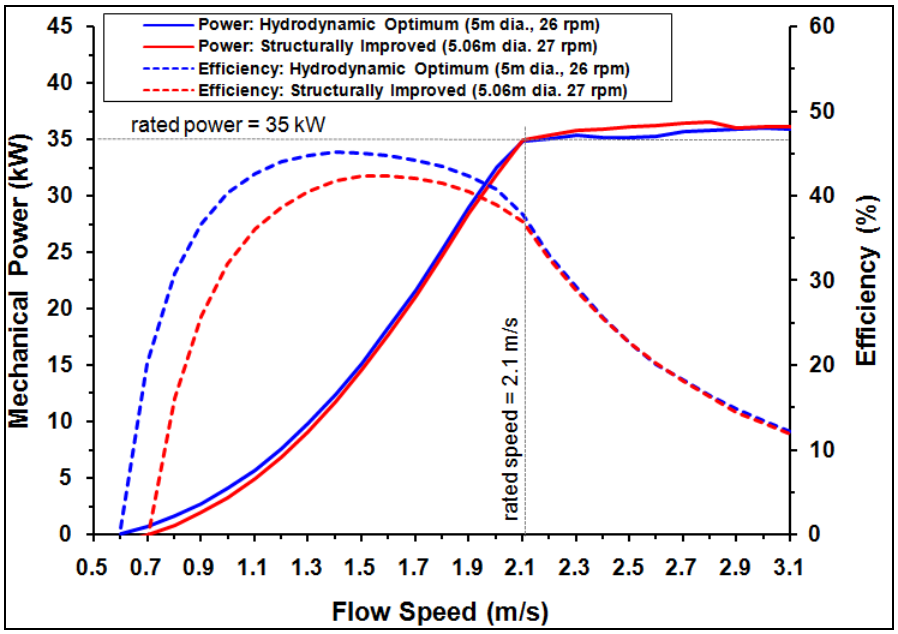

Figure 8 – Power and Efficiency curves for the “Hydrodynamic Optimum” and “Structurally Improved” rotors.

Figure 9 is a comparison of the predicted root flap bending moment of the “Hydrodynamic Optimum” and “Structurally Improved” blade shapes. The “Structurally Improved” shape is subject to a slightly higher flap bending moment at the root due mostly to its larger radius. However, the difference is small relative to the magnitudes of the moments.

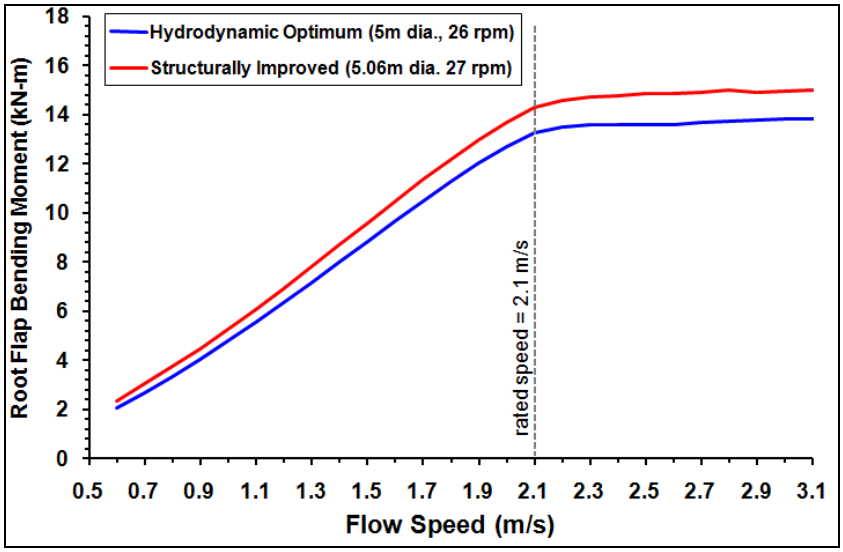

Figure 9 – Comparison of root flap bending moments for the “Hydrodynamic Optimum” and “Structurally Improved” rotors.

The flap bending moment is used as the basis of comparison because it is significantly larger than the edge bending moment over the entire range of flow speeds. The ratio of the root flap bending moment to the root edge bending moment is plotted as a function of flow speed in Figure 8. At low flow speeds, the edge moment which drives the rotation of the blade is near zero while the flap bending moment remains a positive number. This drives the ratio to be very high at low flow speeds. At higher flow speeds, this ratio converges on a value of approximately 4:1 as the blade operates into deep stall.

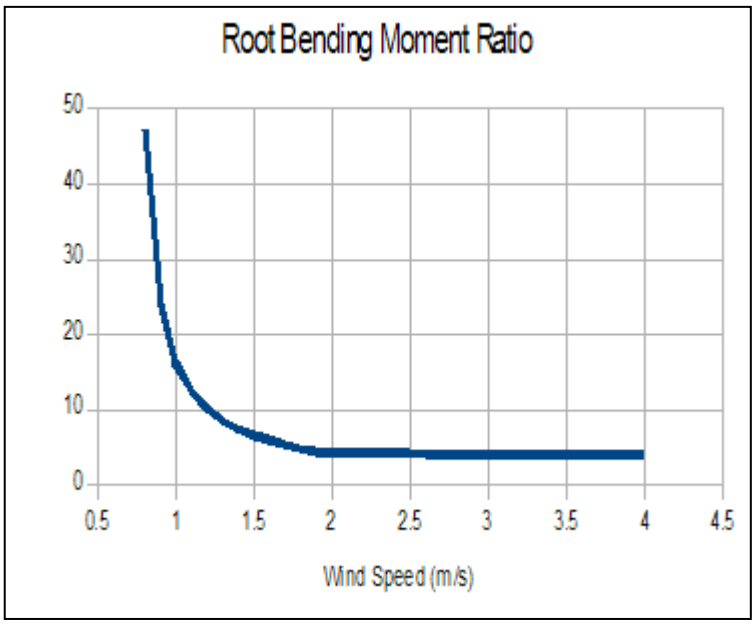

Figure 10 – Root Bending Moment Ratio for Structurally Optimized Blade

5. STRUCTURAL ANALYSIS

Using the hydrodynamically optimized blade shape (chord, twist, and hydrofoil distributions) and the steady state hydrodynamic loads for three separate blade shapes, the structural team was able to determine the properties for blades composed of both composite and solid material. Using these properties, a structural analysis was performed to ensure that the final blade designs could withstand the stresses they will encounter.

5.1 Moment Calculations

The first step of the structural design process was to calculate the necessary force and moment distributions along the span of the blade, so that the stress and strain at each blade station can be calculated. Figure 11 shows the diagram of an arbitrary blade cross section from which the expressions to calculate the forces were derived.

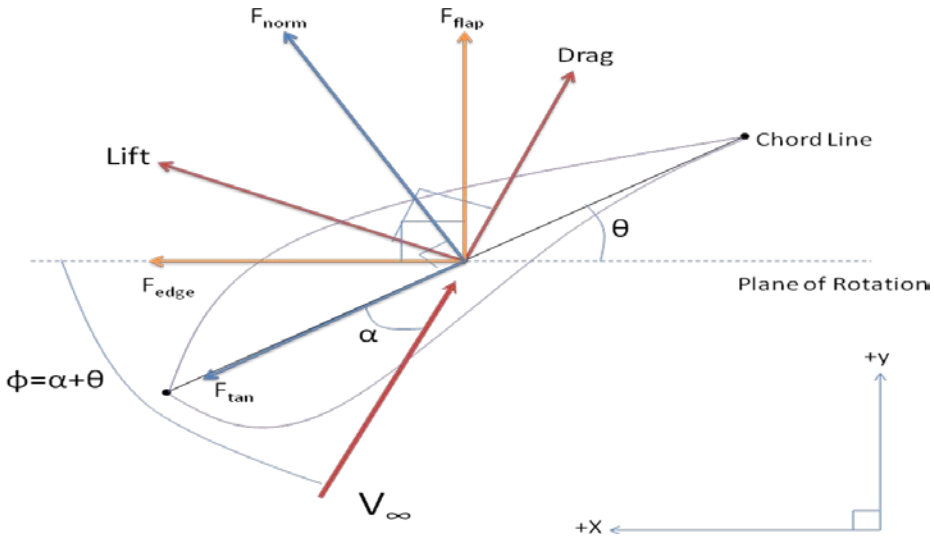

Figure 11: Blade cross-section diagram used to derive forces.

Using Figure 11, the lift and drag forces may be transformed into the needed tangential and normal forces which are in alignment with the airfoil geometry. In order to do this, the lift and drag forces may be found using equations 8 and 9. The values for these forces were determined from the WT_Perf program output provided by the hydrodynamic team.

$$Lift = L = \frac{1}{2}\rho V_{loc}^2 c\Delta r C_l \tag{8}$$

$$Drag = D = \frac{1}{2}\rho V_{loc}^2 c\Delta r C_d \tag{9}$$

Next, the forces in the normal and tangential directions along with the flapwise and edgewise directions could be found by multiplying by the components of the lift and drag forces. The normal and tangential forces are determined in equations 10 and 11 using the angle of attack, α. Similarly, the flapwise and edgewise forces are determined in equations 12 and 13 using the sum of the angle of attack and the twist angle, θ.

$$F_{norm} = Lcos(\alpha) + Dsin(\alpha) \tag{10}$$

$$F_{tan} = Lsin(\alpha) - Dcos(\alpha) \tag{11}$$

$$F_{flap} = Dsin(\emptyset) + Lcos(\emptyset) \tag{12}$$

$$F_{edge} = Lsin(\emptyset) - Dcos(\emptyset) \tag{13}$$

Once the necessary forces were calculated, the bending moments in the normal and tangential directions at each station can be calculated. This process is shown in equations 14 and 15 whose variable components are depicted in Figure 12.

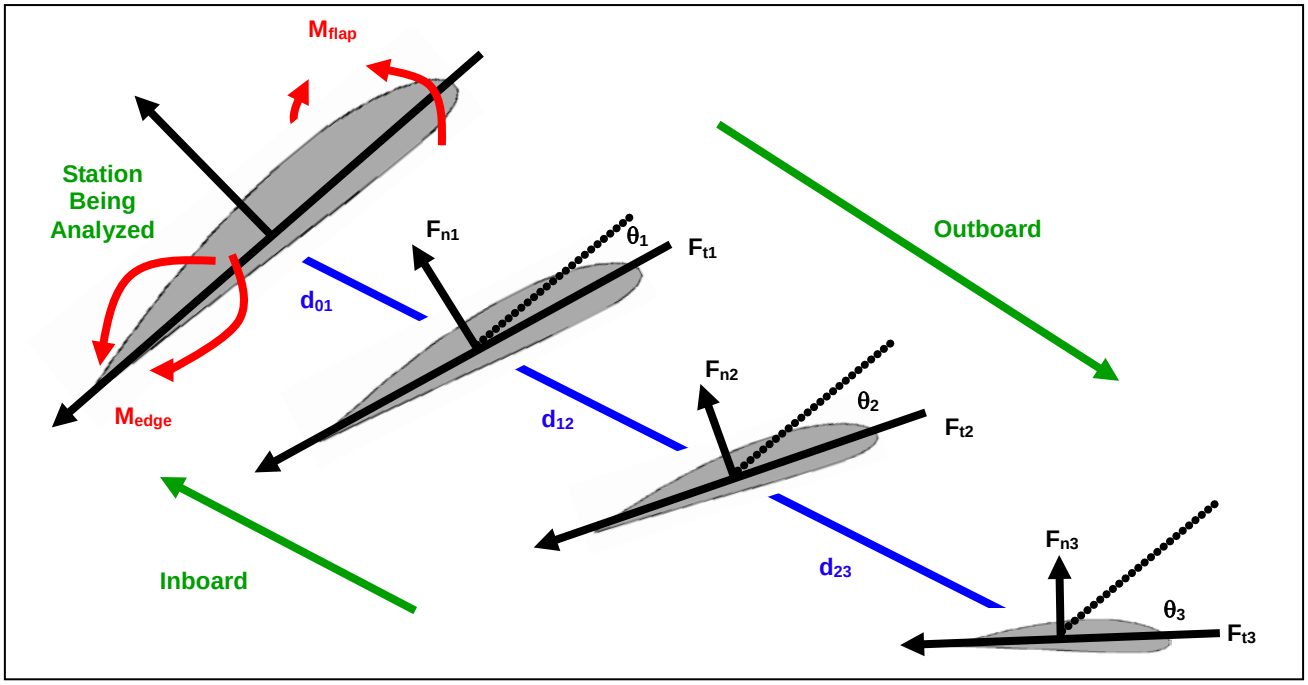

Figure 12. Diagram used to calculate normal and tangential moments at each blade station.

$$M_{norm} = \left[F_{n1}\cos(\theta_1) + F_{t1}\sin(\theta_1)\right]\times\left[d_{01}\right] + \left[F_{n2}\cos(\theta_2) + F_{t2}\sin(\theta_2)\right]\times\left[d_{01} + d_{12}\right] + \left[F_{n3}\cos(\theta_1) + F_{t31}\sin(\theta_3)\right]\times\left[d_{01} + d_{12} + d_{23}\right] \tag{14}$$

$$M_{\tan} = \left[F_{n1}\sin(\theta_1) + F_{t1}\cos(\theta_1)\right]\times\left[d_{01}\right] + \left[F_{n2}\sin(\theta_2) + F_{t2}\cos(\theta_2)\right]\times\left[d_{01} + d_{12}\right] + \left[F_{n3}\sin(\theta_1) + F_{t31}\cos(\theta_3)\right]\times\left[d_{01} + d_{12} + d_{23}\right] \tag{15}$$

As the diagram and equations show, the resultant moment at each station simply becomes the sum of the contributions of each of the forces on all stations outboard of the station being analyzed, rotated to the local coordinate

system of the station being analyzed, and multiplied by the radial distance of each outboard station. The moments were then multiplied by a factor of 1.1 in order to work a safety factor into the calculations. With these equations, the force in all directions is now known as well as the normal and tangential bending moments at each station, and enough information is now available to begin the structural design and analysis.

5.2 Tier 1 Methodology

The first program developed by the structural team looked at blades composed of solid materials. In order to determine the necessary properties for these types of blades, a sectional based analysis calculating the necessary maximum modulus of elasticity for different stations along the length of the blade was implemented. To do this, several parameters were determined at each radial position along the length of the blade using equations taken from openly available online courseware from the Massachusetts Institute of Technology [10]. The equations shown in this section of the report were all applied in MATLAB to reach the needed results.

First, it was necessary to determine the centroid axis and the area moment of inertia for each airfoil cross-sectional station along the length of the blade. To do this, integration was conducted using equations 16, 17, and 18 shown below. The variables shown in these equations may be seen in Figure 13. Equation 16 is used to find the area of the entire airfoil section by integrating the difference between the highest and lowest point across the length of the blade. Then, the centroid axis is found by integrating the difference between the squares of the upper and lower coordinates of the airfoil section and dividing by twice the area value determined from equation 16. This process is shown in equation 17. Finally, the area moment of inertia for the cross section may be determined using equation 18. In equation 18, the difference between the lower coordinate and the centroid axis is cubed and subtracted from the cubed difference between the upper coordinate and the centroid axis. These values are then integrated over the length of the blade and divided by three. All of the integration performed within MATLAB was conducted using the trapezoid rule for integration.

$$A = \int_0^c \left[Z_u - Z_l \right] dx \tag{16}$$

$$\bar{z} = \frac{1}{2A} \int_0^c \left[{Z^2}_u - {Z^2}_l \right] dx \tag{17}$$

$$I = \frac{1}{3} \int_0^c \left[\left(Z_u - \bar{z} \right)^3 - \left(Z_l - \bar{z} \right)^3 \right] dx \tag{18}$$

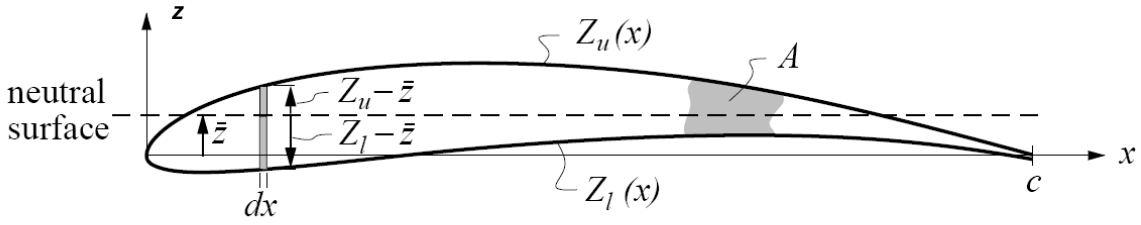

Figure 13 – Bending Inertia of Airfoil Sections Diagram

Next, it is necessary to determine z, the largest distance from the centroid axis to the outer surface of the airfoil section. In order to do this, the maximum value of the difference between the upper surface and the centroid and the lower surface and the centroid must be found using equation 19.

$$z = \max(Z_u - \bar{z}, \bar{z} - Z_l) \tag{19}$$

After z is found, it is then possible to determine the maximum allowable modulus of elasticity for each airfoil section. This is done by utilizing the maximum bending stress equation shown below as equation 20. In this equation, the stress is found by multiplying the normal moment at the section by the maximum distance z and dividing by the moment of inertia. This will be the maximum bending stress because it utilizes the maximum distance from the centroid.

$$\sigma = \frac{Mz}{I} \tag{20}$$

Since the maximum strain value is accepted to be 3000 microstrain for this type of design, it was then possible to manipulate the stress and strain equation 21 and 22 to get an equation that dictates the minimal acceptable value of the modulus of elasticity for a given airfoil section. This equation is a function of already determined moment, z, and the area moment of inertia for the section and may be seen below as equation 23.

$$\sigma = E\varepsilon \tag{21}$$

$$\varepsilon = \frac{Mz}{IE} < 3000\mu\varepsilon \tag{22}$$

$$E > \frac{Mz}{I\varepsilon} = \frac{Mz}{0.003I} \tag{23}$$

Finally, the calculated minimum values for the modulus of elasticity were plotted against their radial position down the length of the blade for two separate blades. The findings of this procedure may be seen in the Tier 1 Results section of this report.

5.3 Tier 2 Methodology

The structural analysis also required a program capable of analyzing the properties of the blade shapes using composite lamina shells rather than solid material. This program was called Tier 2 and once again implemented MATLAB programming code. Although many of the final properties of the structure were determined using equations defined in MATLAB, the primary composite information was found using an outside analytical program called PreCOMP (Pre-processor for computing composite blade properties) [11]. PreCOMP is capable of taking lamina layer input for a vector of radial blade stations along the length of the blade and returning structural properties for the individual stations. The results of PreCOMP were then manipulated to find the maximum bending stress and strain in four different directions at each blade station. While these properties will only be approximate, they will provide enough information to select a group of composite materials that will be appropriate for our application.

In order for PreCOMP to determine the structural properties for the different composite airfoil cross sections, it requires input describing the lay-up and lamina structure of the composite materials to be modeled. For our purposes, this would have required manipulating a total of seventy different hand typed text files for each individual run of the program. Rather than writing these files for each individual lamina setup, a single excel spreadsheet was used to manipulate the numbers in a much more efficient way. The excel spreadsheet contained all of the information on the composite material including: the number of laminas, the number of plies and their thicknesses, and the material in each lamina for both the outside composite layer and the webs at each individual blade station. MATLAB was used to read the single excel file and then write the information into the individual structural lay-up files for each station. These files were then used in conjunction with other text files containing information on the materials properties, overall blade shape, and airfoil shapes. These files were left out of the excel spreadsheet because their information could not be changed, while the composite structure information was purposefully altered between program runs to get the required results.

Once MATLAB had written all of the needed input files for PreCOMP, the code was used to run PreCOMP, and the text file output was once again read into MATLAB for further manipulation. The output of PreCOMP is diverse and useful; however, only the data for shear center and stiffness were used for determining the structural properties. A diagram containing most of the variables used for the stress and strain calculations may be seen in Figure 14.

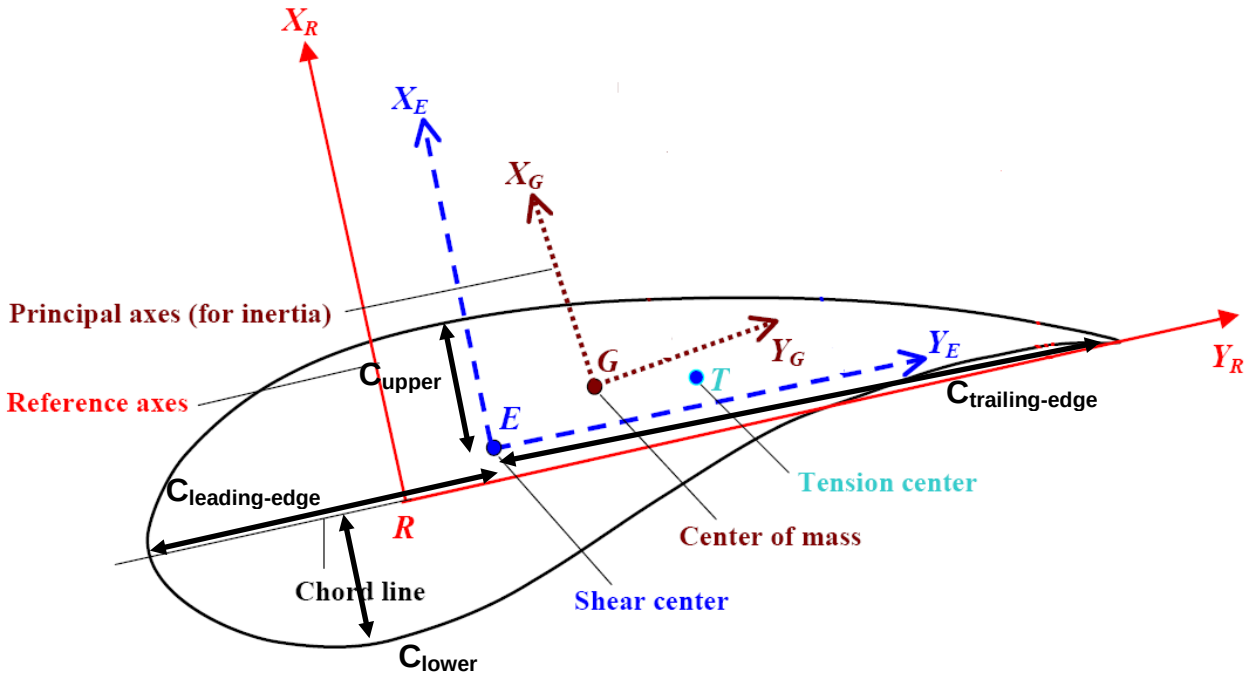

Figure 14 – Reference Diagram for PreCOMP Information

PreCOMP gives the stiffness in both the normal direction, about the Y_E axis and the tangential direction about the X_E axis. It also gives the coordinates for the shear center. Using these values along with the Moments in the normal and tangential direction, it is possible to determine the strain in all four directions at each blade station. The procedure for calculating these strain values is shown below in equations 24, 25, 26, and 27. Equation 24 defines the maximum strain above the chord line. It is found by multiplying the moment in the normal direction at this point by the distance between the shear center and the upper most airfoil data point and then dividing by the stiffness in the normal direction. Likewise, equation 25 is used to find the maximum strain in the normal direction below the chord line by multiplying by the distance between the shear center and the lowest airfoil coordinate rather than the highest. Equation 26 and 27 show the same formula for the tangential direction. Equation 26 defines the strain at the leading edge of the airfoil and equation 27 defines the strain at the trailing edge.

$$\varepsilon_{upper} = \frac{M_{norm} c_{upper}}{IE_{norm}} \tag{24}$$

$$\varepsilon_{lower} = \frac{M_{norm} c_{lower}}{IE_{norm}} \tag{25}$$

$$\varepsilon_{leading-edge} = \frac{M_{\tan} c_{leading-edge}}{IE_{\tan}} \tag{26}$$

$$\varepsilon_{trailing-edge} = \frac{M_{\tan} c_{trailing-edge}}{IE_{\tan}} \tag{27}$$

After the strains in the four directions are found, it is then possible to find the stress in all four directions using the stress-strain equation shown in equation 28. In this equation, each strain value is simply multiplied by the generally accepted modulus of elasticity for a fiberglass composite material of this type, taken to be approximately 27.6 gigapascals.

$$\sigma = E\varepsilon \tag{28}$$

Finally, the stress and strain values were plotted against their radial position down the length of the blade. The strain values were also plotted with a value of 3000 microstrain, the maximum stress limit for the composite material. If the blade composite material experienced more then 3000 microstrain at a given point, it was unacceptable and had to be strengthened by increasing lamina thickness or the number of plies in that area.

5.4 Tier 1 Results

The results from the Tier 1 analysis of both the thin NACA blade and hydrodynamically optimized FFA blade are shown in Figure 15.

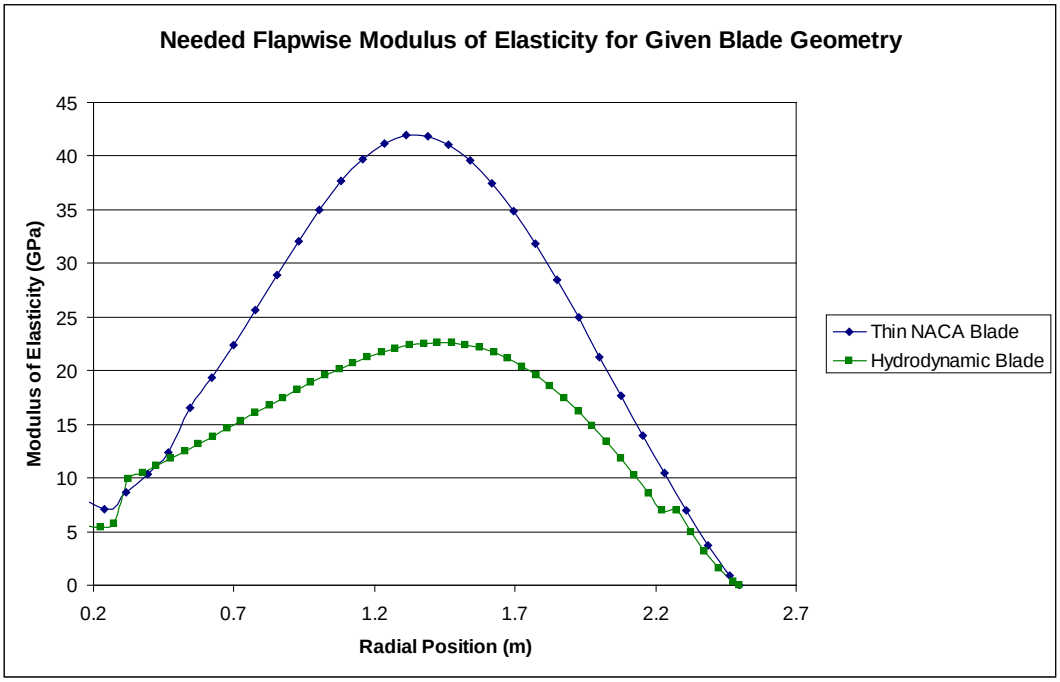

Figure 15: Required normal direction modulus of elasticity for both the NACA blade and the Hydrodynamically optimized FFA blade. The flow conditions are 26 rpm and 3.1 m/s.

Both blade shapes appear to have the highest required modulus of elasticity around the same radial position while maximum required value for the modulus is significantly higher for the NACA blade than the FFA blade. This is likely due to the fact that the FFA blade is much thicker in general than the NACA blade, and thus there is more material to help absorb the bending stresses.

From the figure, the highest required modulus of elasticity was ~42 GPa and ~23 GPa for the NACA blade and the FFA blade respectively. Both of these values seem to be very attainable for a solid carbon fiber blade. When you consider that the FFA blade has better hydrodynamic performance and requires a material with a realistic stiffness value, it seems that the solid carbon fiber FFA blade without a circular root would be the ideal candidate as a final design.

5.5 Tier 2 Results

A final layup for the composite structure blade was chosen through a “trial and error” optimization method where the layup was modeled after the "Design of 9-Meter Carbon-Fiberglass Prototype Blades" on the Sandia website [12]. After using the carbon-fiberglass blade as a starting point, the composite was fine tuned in several ways. The team decided to use only fiberglass materials with approximately 80% of the material in the axial direction and 20% at a 45 degree angle. The number of plies at each blade station was chosen with both the 80% ratio and a maximum total composite thickness in mind. This was especially important since the initial testing led to a composite layer over half the size of the blade thickness, while the PreCOMP computations assume that the composite layers are relatively thin with reference to the thickness of the blade. In addition, ply drops were all greater than a quarter of the local chord length from each other. Finally, only fiber-glass materials were used and a strain limit of 3000 microstrain was upheld. After running the Tier 2 program several times, a final layup design was decided. This layup is defined below in Figure 16 and Table 1. Similar results were found with and without webs; therefore, no webs were used in the composite design. One possible

explanation for the negligible effect of webs is the small size of the blade compared to large wind turbine blades.

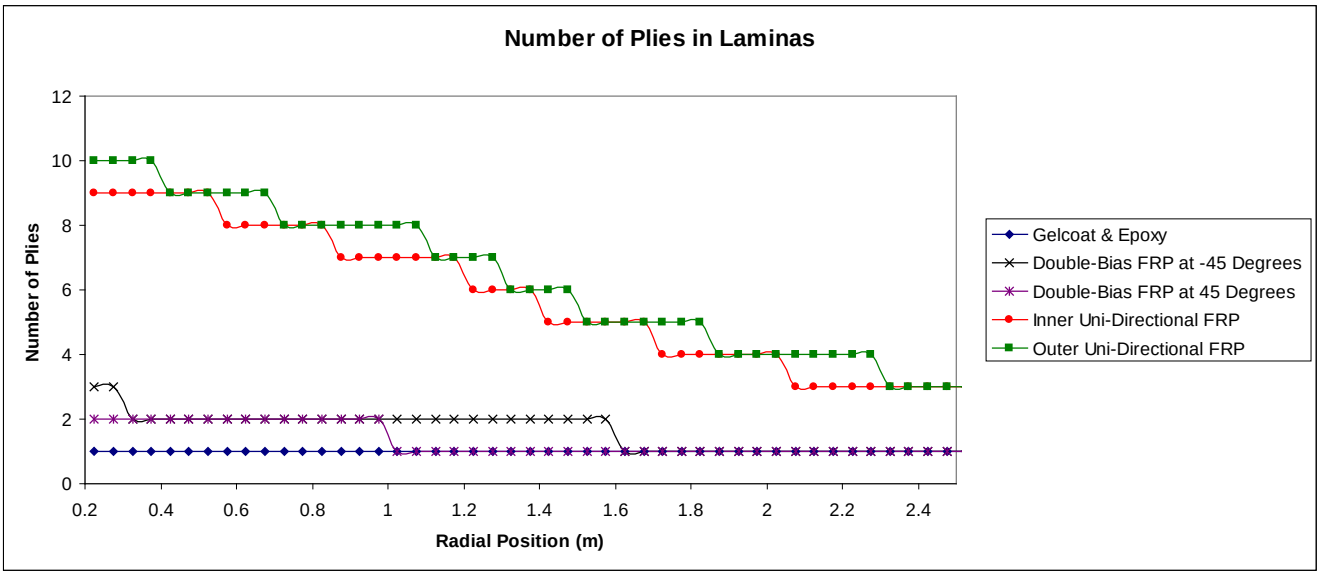

Figure 16: Final Layup Design Ply Count by Radial Position

Table 1: Final layup design laminate schedule for circular root, FFA turbine blade at 27 rpm and 3.1 m/s

Material Name	E_1 (GPa)	E_2 (GPa)	G_{12} (GPa)	v_{xy}	Density (kg/m^3)	Ply Thickness (mm)
Gel Coat	10E-9	10E-9	1E-9	0.30	1830	0.13
Fill Epoxy	2.41	2.41	0.96	0.30	1154	0.5
Uni-Directional FRP	37.0	9.0	4.0	0.28	1860	0.5
Double-Bias	10.3	10.3	8.0	0.3	1830	0.5
Double-Bias	10.3	10.3	8.0	0.3	1830	0.5
Uni-Directional FRP	37.0	9.0	4.0	0.28	1860	0.5

The layup is defined again in Figure 17. However, this time the plot shows the thickness of each individual lamina layer rather than the number of plies. It also shows the percent of the composite material oriented axially down the length of the blade. As intended, this percentage remains close to 80% throughout the blade with a high of 84% and a low of 75%.

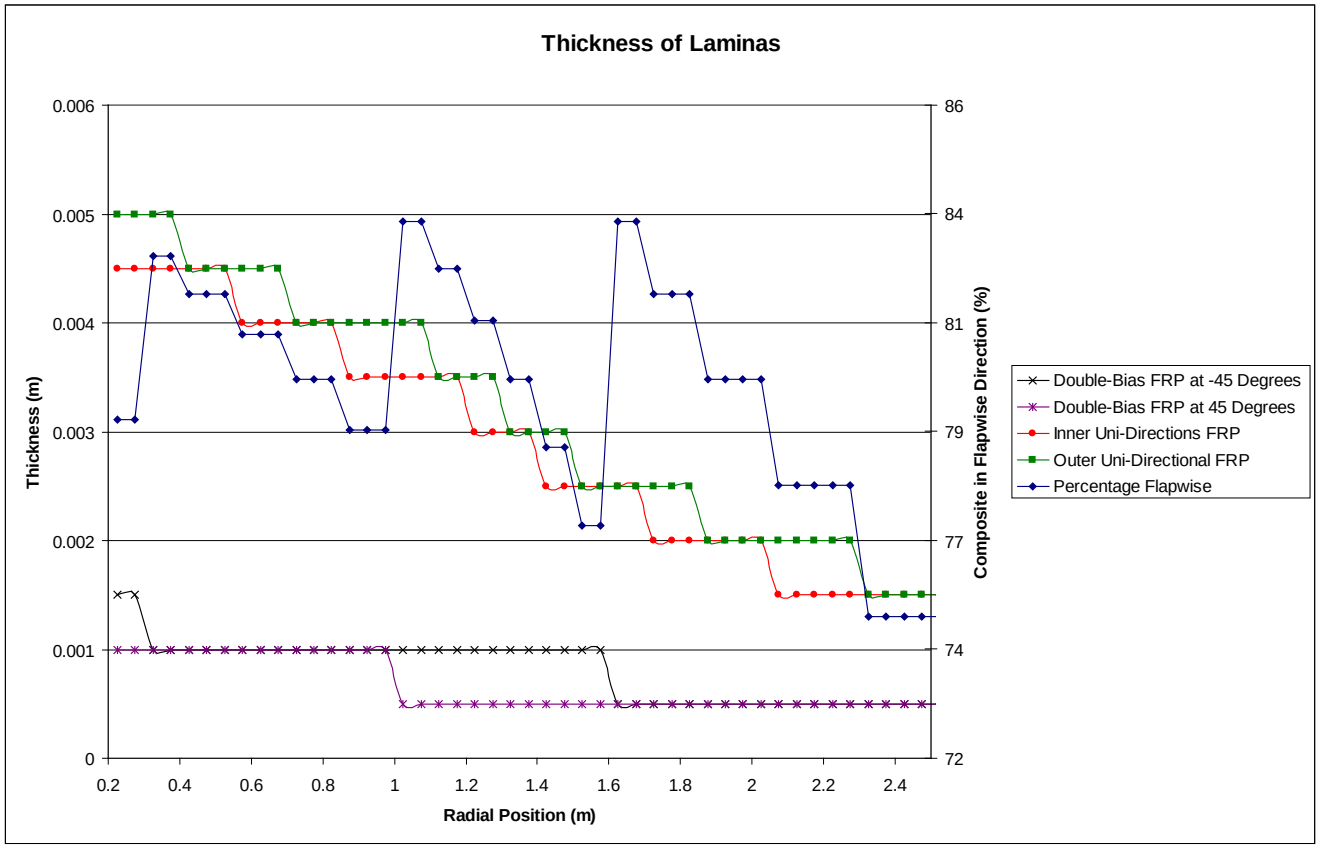

Figure 17: Thickness of each lamina as a function of radial position.

Next, Figure 18 shows the total thickness of the composite materials and the blade. It also depicts the ratio of the composite layer thickness to the total blade thickness. This value represents the percentage of the blade that is made up of the composite material. For our design, the percent total thickness of the composite to the blade approaches 12% on the top and bottom which means almost 24% of the cross section is composed of composite at the thickest part of the airfoil cross section. At the tip of the blade, this value quickly increases to 100%. However, it is believed that 12% of the total thickness is still reasonably thin, and therefore the PreCOMP values are relatively accurate.

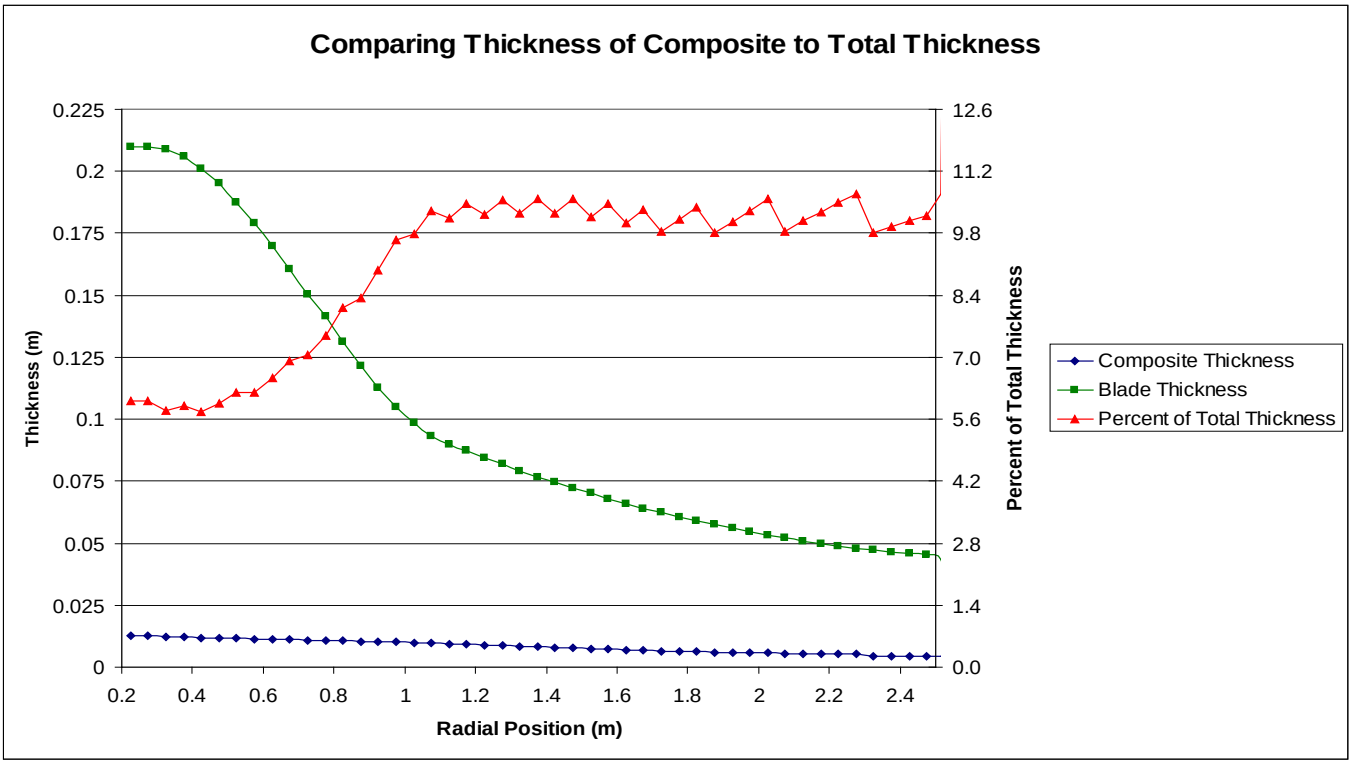

Figure 18: Composite thickness, total thickness and percent total thickness as a function of radial position.

Finally, Figures 19, 20, and 21 show the moment distribution, the stress distribution and the strain distributions for the composite blade respectively. From the figures, it is clear that the designed composite does indeed meet the strain based design requirements with a maximum strain of roughly 2500 microstrain, a value significantly lower than the maximum 3000 microstrain. Furthermore, the plots show the effect of decreasing ply count down the length of the blade through jagged edges on the stress and strain curves. These are to be expected in this type of station based design, and should be more continuous in a manufactured blade. The general curve shown in the stress and strain plots was also expected. As the moment increases from the end of the blade at 2.53 meters inward toward a radial position of 1.5 meters, the stress and strain curves become greater. However, at this point the moment increase slows down and the chord length and composite thickness increase causing the stress and strain curves to have a local maximum and begin decreasing. This decrease in stress and strain continues until a radial position of approximate 0.6 meters is reached. At this point, the chord length greatly decreases while the moment is still increasing. This causes the stress and strain to increase again. However, at this point the blade transitions from an airfoil shape into thick circular root causing a large increase in thickness which in turn limits the increase of stress and strain shown on the diagrams.

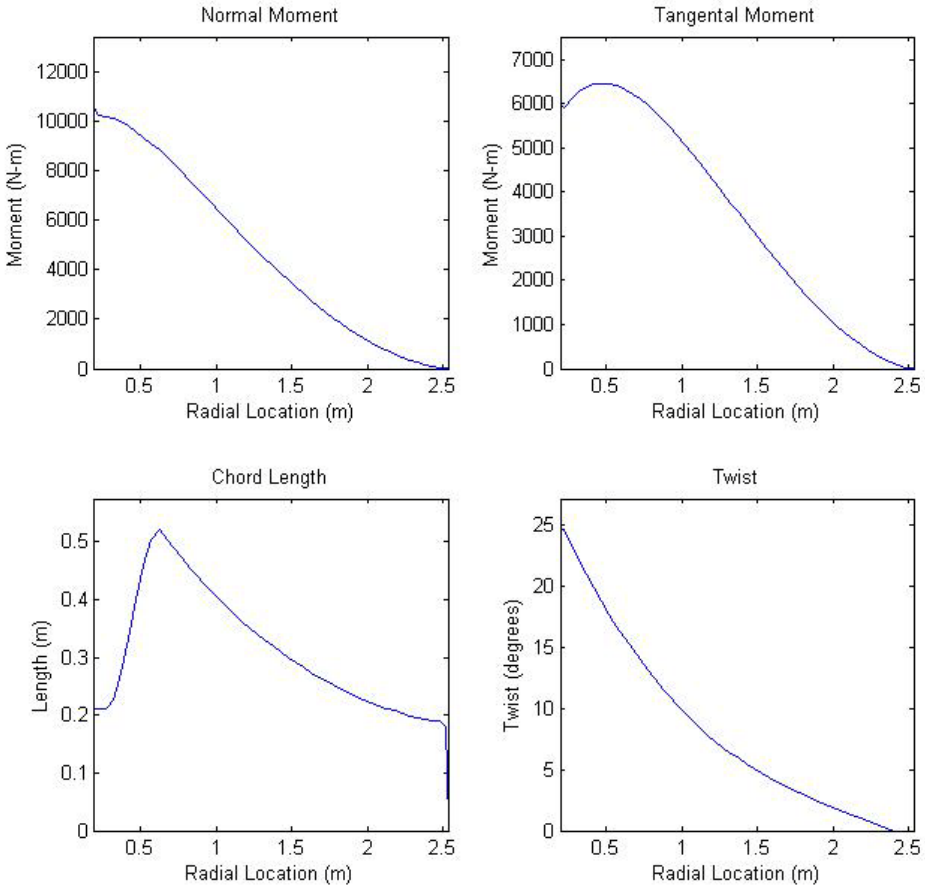

Figure 19: Blade moments as well as some geometry information.

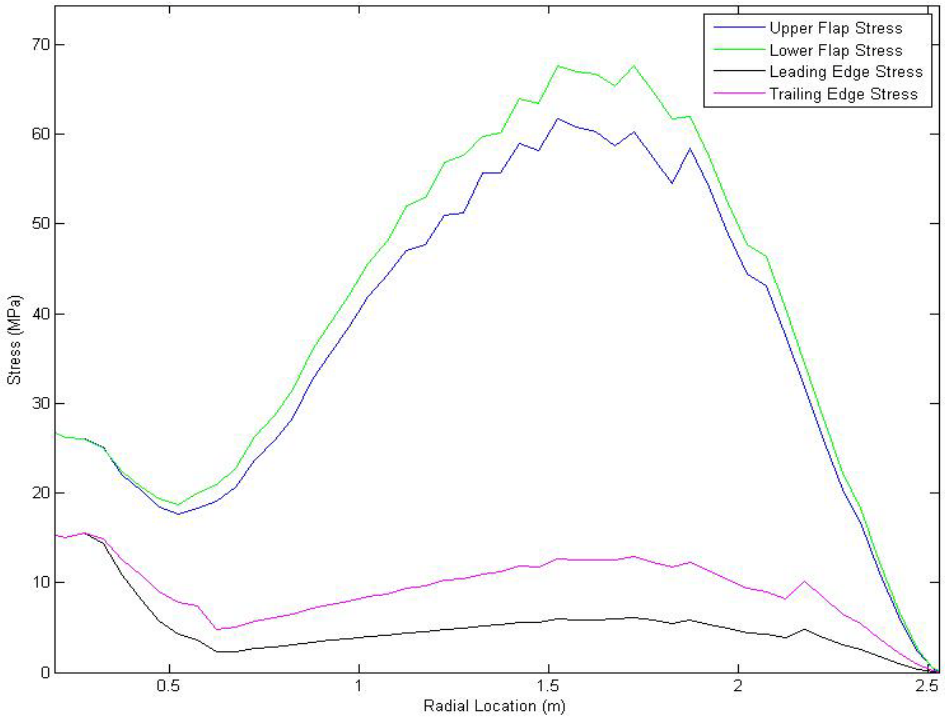

Figure 20: Stress in the normal and tangential directions and a function of radial position.

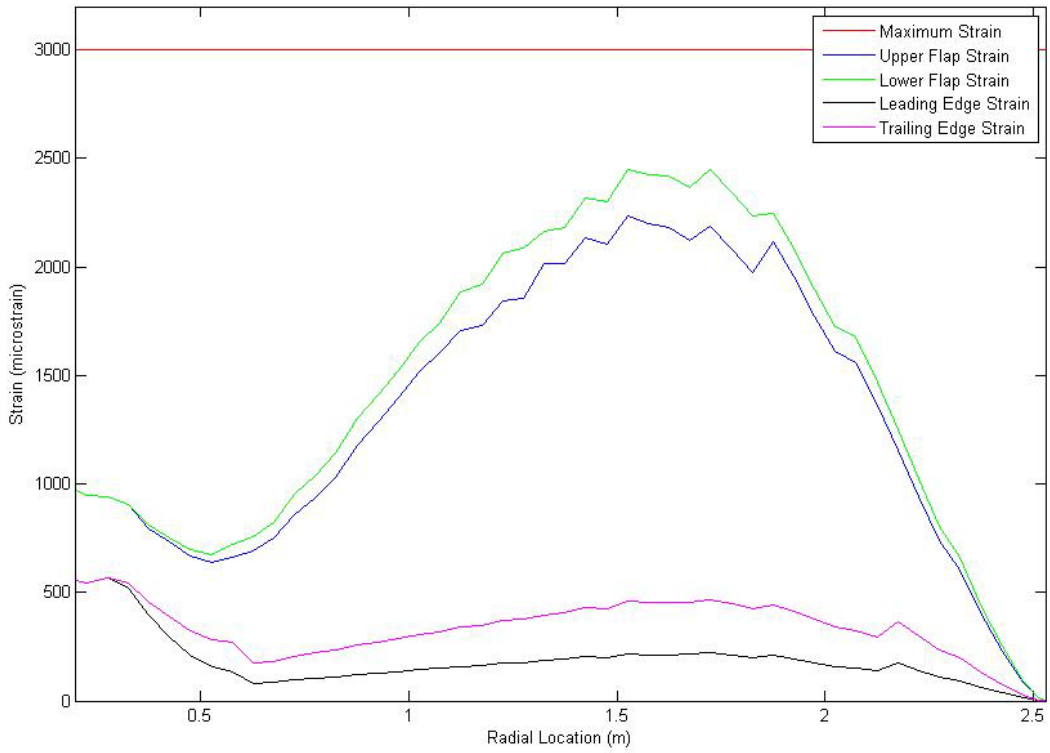

Figure 21: Strain in the normal and tangential direction as a function of radial position.

The final result of the tier 2 program is a calculation of the maximum deflection along the flapwise direction of the blade. The deflection of the blade at 3.1 m/s and 27 rpm is shown in Figure 22. With a tip deflection of only 8 cm, the deflection is not a major design concern and can be neglected. This is especially true since the project specified the blade as part of a downstream turbine. The small deflection is likely a by-product of the strain based design approach taken during this project.

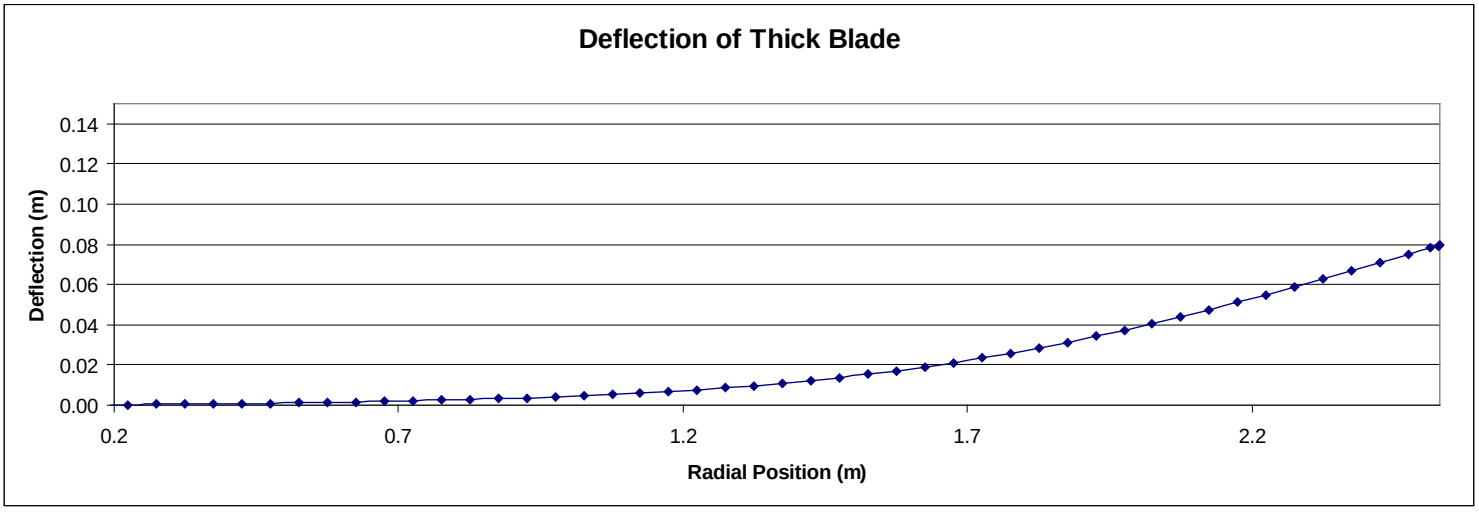

Figure 22: Deflection of the circular root, FFA Turbine blade at 27 rpm and 3.1 m/s.

5.6 NuMAD Modeling

After the composite material was modeled analytically using PreCOMP, the finite element software NuMAD [13] was going to be used in conjunction with ANSYS to calculate where the highest stresses are concentrated on the blade and if they exceed the yield strength of the blade. However, very little analysis could be done on this part of the project due to

the late acquisition of the ANSYS software. Since ANSYS has already been purchased by the University of Tennessee, it could be favorable for the University and NREL to work together on future senior design projects in this area of study.

6. FABRICATION OF BLADE PLUG

At the beginning of the Fall semester, the required “hands-on” component of the senior design class had still not been decided upon. Hence, much of the beginning of the semester was spent attempting to design an appropriate experimental test in addition to the conceptual design of a turbine blade. The most attractive concept discussed was a water tunnel or tow tank experiment designed to validate the team’s ability to predict the inception of cavitation for the designed turbine blade. The UT Space Institute and a local Tennessee Valley Authority site had tow tank facilities that could be used, but it was found that the experiment could not be properly scaled to simulate the conditions in which the blade will be exposed. Building a tow tank at the university was another possibility, but parameter scaling, cost, and complexity made this idea unfeasible. After discussing the situation with NREL and advisors at the University of Tennessee, it was decided that an experiment involving cavitation would be excluded.

Rather than experimentation, the fabrication of a scaled model “blade plug” was decided to be the hands-on component of the senior design class. A blade plug is used in the mold making process of mass produced turbine blades. The plug is currently being manufactured using a three-dimensional polymer printer available in the biomedical engineering facilities at the University of Tennessee.

References

[1] M. Buhl, "NWTC Design Codes (WT_Perf by Marshall Buhl.)" [Online document] July 2008, [2008 Dec. 12] Available at HTTP: http://wind.nrel.gov/designcodes/simulators/wtperf/

[2] J.F. Manwell, J.G. McGowan, and A.L. Rogers, Wind Energy Explained, England: John Wiley & Sons Ltd, 2006.

[3] Y. Lecoffre, Cavitation Bubble Trackers, Paris: A.A. Balkema, 1999.

[4] K. Jones, "Kevin's Online Tools: Panel Code Version 2." [Online document], [2008 Dec. 12] Available at HTTP: http://aa.nps.edu/~jones/online_tools/panel2/

[5] S.J. Miley, A Catalog of Low Reynolds Number Airfoil Data for Wind Turbine Applications, College Station, Tex: Texas A&M University, 1982.

[6] I.H Abbott and A.E. Von Doenhoff, Theory of Wing Sections, New York, Dover Publications, 1959.

[7] F. Bertagnolio, N. Sørensen, J. Johansen and P. Fuglsang, "Wind Turbine Airfoil Catalog." [Online document] Aug. 2001, [2008 Dec. 12] Available at HTTP: http://www.risoe.dk/Research/sustainable_energy/wind_energy/projects/Profcat.aspx?sc_lang=en

[8] C. Hansen, "NWTC Design Codes (AirfoilPrep by Dr. Craig Hansen.)" [Online document] Dec. 2005, [2008 Dec. 12] Available at HTTP: http://wind.nrel.gov/designcodes/preprocessors/airfoilprep/

[9] Massachusetts Institute of Technology Open Course Ware - Unified Engineering I. "Area and Bending Inertia of Airfoil Sections." Available at HTTP: http://ocw.mit.edu/NR/rdonlyres/Aeronautics-and-Astronautics/16-01Fall-2005-Spring-2006/7B146C84-83C9-41A9-B458-6EE42A2A50B3/0/spl10b.pdf

[10] American Institute of Aeronautics and Astronautics, "A collection of the 1998 ASME Wind Energy Symposium technical papers: at the 36th AIAA Aerospace Sciences Meeting and Exhibit, Reno, NV, January 12-15, 1998." (9), New York, American Institute of Aeronautics and Astronautics, and American Society of Mechanical Engineers, 1998.

[11] G. Bir, "NWTC Design Codes (PreComp by Gunjit Bir.)" [Online document] July 2008, [2008 Dec. 12] Available at HTTP: http://wind.nrel.gov/designcodes/preprocessors/precomp

[12] D. Berry, "Design of 9-Meter Carbon-Fiberglass Prototype Blades: CX-100 and TX-100," [Online document] September 2007, [2009 Apr. 23] Available at HTTP: http://www.prod.sandia.gov/cgi-bin/techlib/access-control.pl/2007/070201.pdf

[13] D. Laird, "Sandia National Laboratory (NuMAD by Daniel Liard.)" [Online document] Sept. 2008, [2008 Dec. 12] Available at HTTP: http://www.sandia.gov/wind/NuMAD.htm

[14] M. Buhl, "A New Empirical Relationship between Thrust Coefficient and Induction Factor for the Turbulent Windmill State." [Online document] Aug. 2005, [2008 Dec. 12] Available at HTTP: http://www.nrel.gov/docs/fy05osti/36834.pdf

Appendix A – Governing Equations of BEM & WT_Perf Algorithm

The following section outlines the algorithm and governing equations of BEM theory used by WT_Perf v3.10 to model the hydrokinetic turbine.

Through an iterative process, the goal is to define a flow field at the rotor plane, characterized by the axial induction factor, *a*, and tangential induction factor, *a'*. With initial guesses for *a* and *a'* at each blade element, the iterative solution begins with calculating the velocity components. The normal, tangential, and total relative velocity components are calculated via Equations 1, 2, and 3 respectively.

$$V_{norm} = V_{\infty}(1-a) \quad (1)$$

$$V_{\tan} = (r\,\Omega)(1+a') \quad (2)$$

$$V_{rel} = \sqrt{(V_{norm}^2 + V_{\tan}^2)} \quad (3)$$

The inflow angle, φ, is calculated via Equation 4.

$$\tan(\phi) = \frac{V_{norm}}{V_{\tan}} \quad (4)$$

The Prandtl tip loss model is used to estimate the influence that vortices shed from the blade tips into the wake have on the induced velocity field in the rotor plane. These tip vortices create helical flow structures in the rotor wake, and have a pronounced effect on the power extracted near the tips of the blades. Equations 5, 6, and 7 account for the tip losses near the blade tip, blade hub, and also their combined effect.

$$F_{tip} = \frac{2}{\pi}\cos^{-1}\left[e^{-\frac{B}{2}\frac{R-r}{r\sin\phi}}\right] \quad (5)$$

$$F_{hub} = \frac{2}{\pi}\cos^{-1}\left[e^{-\frac{B}{2}\frac{r-R_{hub}}{R_{hub}\sin\phi}}\right] \quad (6)$$

$$F = F_{tip}F_{hub} \quad (7)$$

With the inflow angle and section pitch angle known (θ_p defined by the blade geometry), the section angle of attack, α, can be calculated from Equation 8.

$$\alpha = \phi - \theta_p \quad (8)$$

The Reynolds number, see Equation 9, uses the blade chord, *c*, as the characteristic length and the total relative velocity, V_{rel}, as the characteristic velocity.

$$Re_c = \frac{V_{rel}\,c}{\nu} \quad (9)$$

WT_Perf determines the local thrust coefficient using Equation 10. The values of the lift and drag coefficients, C_l and $C_{d,}$, are both a function of angle of attack and Reynolds number. The lift and drag coefficients are also dependent on the type of airfoil being used. WT_Perf requires the user to define an airfoil table for each blade section, consisting of lift and drag coefficients as a function of angle of attack and Reynolds number. Having already calculated α and Re_c, WT_Perf extracts the values of C_l and C_d from these airfoil tables at every iteration.

$$C_T = \frac{\sigma'(1-a)^2(C_l\cos\phi + C_d\sin\phi)}{\sin^2\phi} \quad (10)$$

The axial and tangential induction factors, a and a' are now updated for the next iteration. If $C_T \leq 0.96F$, then Equation 11 is used to update the axial induction factor.

$$a = \left[1 + \frac{4F \sin^2 \phi}{\sigma' (C_l \cos \phi + C_d \sin \phi)} \right]^{-1} \tag{11}$$

Now, if $C_T > 0.96F$, the blade element is highly loaded and a modified Glauert correction is used to update the axial induction factor, see Equation 12. This modification to the Glauert empirical relation, derived by Marshall Buhl [14], includes tip loss corrections. The tangential induction factor is updated using Equation 13.

$$a = \frac{18F - 20 - 3\sqrt{C_T(50 - 36F) + 12F(3F - 4)}}{36F - 50} \tag{12}$$

$$a' = \left[\frac{4F \sin \phi \cos \phi}{\sigma' (C_l \sin \phi - C_d \cos \phi)} - 1 \right]^{-1} \tag{13}$$

WT_Perf repeats this iterative process for each blade element, starting again with Equation 1 through Equation 13. The final values of the axial and tangential induction factors are reached once the newest induction factors are within an acceptable tolerance of the previous iterations.

Once this iterative process is complete and the induction factors have been solved for at every blade element, the differential torque element can be calculated at every radial element along the blade via Equation 14.

$$dQ = \sigma' \pi \rho \frac{V_\infty^2 (1 - a)^2}{\sin^2 \phi} (C_l \sin \phi - C_d \cos \phi) r^2 dr \tag{14}$$

Finally, the total power extracted from the moving fluid by the turbine rotor is given by Equation 15.

$$P = \int_{r_{hub}}^{R} \Omega \, dQ \tag{15}$$

Appendix B – List of Variables Used

C_{Pmin} = minimum pressure coefficient (note: C_{Pmin} is a function of angle of attack)
Cp = power coefficient
P_{atm} = absolute atmospheric pressure (101,325 Pa at sealevel)
P_V = vapor pressure of water (approximately 2,500 Pa for sea-water)
ρ = water density (approximately1025 kg/m^3 for sea-water)
g = gravitational constant (9.81 m/s^2)
h = depth from the free surface to the point of interest on the blade
a = axial induction factor
a' = tangential induction factor
λ = tip speed ratio
V_∞ = free stream velocity
V_{norm} = axial induced velocity
V_{tan} = tangential induced velocity
V_{rel} = total relative induced velocity
F_{tip} = tip loss factor at the blade tip
F_{hub} = tip loss factor at the blade root
F = total tip loss factor
r = local radius
R = blade radius
R_{hub} = radius of the hub (i.e. radius to the blade root)
B = number of blades
α = angle of attack (angle between the airfoil chord line and the vector representing V_{rel})
φ = inflow angle (angle between the plane of rotation and the vector representing V_{rel})
θ_p = blade pitch angle (angle between the airfoil chord line and the plane of rotation. Note: this can be referenced from different locations along the blade such as the tip or r/R = 0.75)
Re_c = non-dimensional Reynolds number, using the chord length as the characteristic length
c = chord length
υ = kinematic viscosity
C_l = non-dimensional lift coefficient
C_d = non-dimensional drag coefficient
C_T = non-dimensional thrust coefficient
$\sigma' = \frac{Bc}{2\pi r}$ = local solidity
dQ = differential torque element
dr = differential radius element
P = total power extracted from the moving fluid
Ω = rotational speed of the rotor
L = lift force
D = drag force
V_{loc} = local velocity
F_{norm} = force normal to chord line
F_{tan} = force tangential to chord line
F_{flap} = force normal to hub plane
F_{edge} = force tangential to hub plane
M_{norm} = moment about chordline at each blade station
M_{tan} = moment about X_E reference plane at each blade station
A = area of airfoil at each blade station

$\bar{z}$ = centroid axis distance from chord line
I = area moment of inertia of airfoil cross section
Z_u = upper coordinates of airfoil cross section
Z_l = lower coordinates of airfoil cross section
z = maximum length from centroid to Z_l or Z_u
σ = bending stress
ε = strain
IE = stiffness about the X_E or Y_E reference plane
E = modulus of elasticity
c = length from shear center to upper, lower, trailing, and leading edge of airfoil shape